

# Does the X–ray emission of the luminous quasar RBS 1124 originate in a mildly relativistic outflowing corona?

G. Miniutti<sup>1\*</sup>, E. Piconcelli<sup>2</sup>, S. Bianchi<sup>3</sup>, C. Vignali<sup>4,5</sup> and E. Bozzo<sup>6</sup>

<sup>1</sup> Centro de Astrobiología (CSIC–INTA); LAEFF, P.O: Box 78, E-28691, Villanueva de la Cañada, Madrid, Spain

<sup>2</sup> INAF–Osservatorio Astronomico di Roma, Via Frascati 33, I–00040, Monteporzio Catone, Italy

<sup>3</sup> Dipartimento di Fisica, Università degli Studi Roma Tre, via della Vasca Navale 84, 00146 Roma, Italy

<sup>4</sup> Dipartimento di Astronomia, Università degli Studi di Bologna, Via Ranzani 1, 40127 Bologna, Italy

<sup>5</sup> INAF–Osservatorio Astronomico di Bologna, Via Ranzani, 1, 40127 Bologna, Italy

<sup>6</sup> INTEGRAL Science Data Center (ISDC), Science Data center for Astrophysics, Ch. d’Ecogia 16, CH–1290 Versoix (Ge), Switzerland

5 November 2018

## ABSTRACT

We have observed the luminous ( $L_{2-10\text{ keV}} \simeq 6 \times 10^{44} \text{ erg s}^{-1}$ ) radio–quiet quasar RBS 1124 ( $z = 0.208$ ) with *Suzaku*. We report the detection of a moderately broad iron (Fe) line and of a weak soft X–ray excess. The X–ray data are very well described by a simple model comprising a power law X–ray continuum plus its reflection off the accretion disc. If the inner disc radius we measure ( $r_{\text{in}} \leq 3.8$  gravitational radii) is identified with the innermost stable circular orbit of the black hole spacetime, we infer that the black hole powering RBS 1124 is rotating rapidly with spin  $a \geq 0.6$ . The soft excess contribution in the 0.5–2 keV band is  $\sim 15$  per cent, about half than that typically observed in unobscured Seyfert 1 galaxies and quasars, in line with the low disc reflection fraction we measure ( $R_{\text{disc}} \simeq 0.4$ ). The low reflection fraction cannot be driven by disc truncation which is at odds not only with the small inner disc radius we infer but, most importantly, with the radiatively efficient nature of the source ( $L_{\text{Bol}}/L_{\text{Edd}} \simeq 1$ ). A plausible explanation is that the X–ray corona is the base of a failed jet (RBS 1124 being radio–quiet) and actually outflowing at mildly relativistic speeds. Aberration reduces the irradiation of the disc, thus forcing a lower than standard reflection fraction, and halves the inferred source intrinsic luminosity, reducing the derived Eddington ratio from  $\simeq 1$  to  $\simeq 0.5$ . A partial covering model provides a statistically equivalent description of the 0.3–10 keV data, but provides a worse fit above 10 keV. More importantly, its properties are not consistent with being associated to the Fe emission line, worsening the degree of self–consistency of the model. Moreover, the partial covering model implies that RBS 1124 is radiating well above its Eddington luminosity, which seems unlikely and very far off from previous estimates.

**Key words:** galaxies: active – X-rays: galaxies

## 1 INTRODUCTION

The X-ray spectrum of unobscured (type I) Active Galactic Nuclei (AGN) is generally dominated by a power law component which most likely comes from Compton up–scattering of the soft UV/EUV photons from the accretion disc in hot active regions (the so–called X–ray corona). This simple spectral description is however almost ubiquitously modified by a soft X–ray excess below 1–2 keV (e.g. Pounds et al. 1987), by the presence of a narrow iron (Fe) emission line at  $\sim 6.4$  keV (e.g. Bianchi et al. 2007), and by partially ionized absorbers in the line of sight (the so–called warm absorbers, see e.g. Blustein et al. 2005). Broad Fe emission lines are

also sometimes observed and generally attributed to X–ray reflection of the primary power law continuum off the accretion disc (e.g. Nandra et al. 2007; Fabian & Miniutti 2009). While the narrow Fe line origin is not highly debated and is most likely associated with reflection from distant matter (such as the obscuring material of AGN unification schemes) and the warm absorber properties can be inferred from the analysis of high resolution spectra, the nature of the soft excess emission is not yet well established.

The soft excess typically rises smoothly above the extrapolation of the 2–10 keV continuum and its shape is suggestive of low temperature ( $kT \sim 150$  eV) Comptonization of the soft disc photons, a much lower electron temperature than that generally invoked to account for the high energy power law component ( $kT \sim 100$  keV). However the “soft excess temperature” is remarkably uniform in radiatively efficient sources despite a large

\* gminiutti@laeff.inta.es

range in black hole mass and hence disc temperatures, casting doubts on this interpretation (see e.g. Walter & Fink 1993; Czerny et al. 2003; Gierlinski & Done 2004; Middleton et al. 2007; Miniutti et al. 2009a). The uniform temperature of the soft excess may have a natural explanation if the soft excess is due to atomic rather than thermal processes. Partially ionized material may produce a uniform soft excess in a relatively wide ionization state range because of excess opacity in the 0.7–2 keV range with respect to neighbouring energy bands. This simple idea leads to two main competing atomic-based interpretations of the soft excess in AGN, namely absorption by partially ionized gas or X-ray reflection from the accretion disc material (see e.g. Gierlinski & Done 2004; Crummy et al. 2006).

High resolution spectroscopy of the soft X-ray spectra of AGN does indeed reveal a series of absorption features, but the associated gas is not able to account for the soft excess (e.g. Blustin et al. 2005 and references therein). Hence, for the absorption interpretation to be consistent with the available data, the predicted sharp absorption features have to be smoothed out by very large velocity smearing such as those expected in fast outflows and winds. However, when physical models are considered, absorbing winds/outflows are able to produce significant soft excesses only by also predicting relatively sharp absorption features in the soft X-rays which are not consistent with the data, casting doubts on the overall interpretation or, alternatively, calling for more complex physical models (Sim et al. 2008; Schurch, Done & Proga 2009). On the other hand, the sharp features associated with the X-ray reflection spectrum are naturally smoothed out by the large orbital velocities of the inner accretion disc, so that no additional physics besides the standard disc/corona structure is required to explain the data in the framework of the disc reflection interpretation of the soft excess (Fabian & Miniutti 2009). The recent detections of broad Fe L and K emission lines and of a reflection time lag in the NLS1 galaxy 1H 0707–495 favour the reflection interpretation in this source, possibly indicating that this is indeed the right interpretation for the soft excess in most cases (Fabian et al. 2009; see also Fabian et al. 2004).

RBS 1124 ( $z = 0.208$ , a.k.a. RX J1231.6+7044) is a broad line quasar (QSO) with  $H\beta$  FWHM of  $4.26 \pm 1.25 \times 10^3 \text{ km s}^{-1}$  and optical luminosity  $\lambda L_{5100} \simeq 1.26 \times 10^{44} \text{ erg s}^{-1}$  (Grupe et al. 2004). The 5100Å luminosity, combined with the  $H\beta$  width, can be used to infer a black hole mass of  $\simeq 1.8 \times 10^8 M_{\odot}$  (e.g. by using the relationships in Vestergaard & Peterson 2006). The bolometric luminosity has been estimated by Grupe et al. (2004) from a combined fit to the optical–UV and X-ray data and is  $L_{\text{Bol}} \simeq 3.4 \times 10^{45} \text{ erg s}^{-1}$  which, together with the black hole mass estimate, implies that RBS 1124 is radiatively efficient with an Eddington ratio of  $\simeq 0.15$ . Note however that, as pointed out in Grupe et al. (2004), the derived bolometric luminosity has to be considered as an estimate only given the lack of EUV data.

In the X-rays, RBS 1124 was detected by ROSAT, and is in the ROSAT All-sky Bright Source Catalogue (Voges et al. 1999) with a RASS 0.2–2 keV flux of  $\sim 7.6 \times 10^{-12} \text{ erg cm}^{-2} \text{ s}^{-1}$  and a spectral shape consistent with a simple power law model absorbed by the Galactic column density (Grupe, Thomas & Beuermann 2001). It is also present in the first release of the *XMM-Newton* Slew Survey Catalogue XMMSL1 (Saxton et al. 2008) with a 0.2–2 keV EPIC-pn count rate of  $\sim 3.9 \text{ cts s}^{-1}$ , corresponding to a flux of  $\sim 6.5 \times 10^{-12} \text{ erg cm}^{-2} \text{ s}^{-1}$  in the same band (assuming an absorbed power law model with  $N_{\text{H}} = 1.5 \times 10^{20} \text{ cm}^{-2}$  and  $\Gamma = 2.38$ , as obtained from the RASS by Grupe et al. 2001).

The relatively high Eddington ratio of RBS 1124 suggests that

its X-ray spectrum may share a series of common properties with the class of Seyfert 1 galaxies, and in particular the source may represent a rare opportunity to observe a soft excess at very high X-ray luminosities. We then decided to observe the source in the widest possible X-ray band by using the Japanese (JAXA/NASA) X-ray observatory *Suzaku* which is sensitive enough (for the given source brightness) to provide accurate spectral information in the  $\sim 0.3$ –30 keV band. Here we present results from a  $\sim 86 \text{ ks}$  *Suzaku* observation of RBS 1124, and we also present for the first time results from *Swift*/XRT observations of the source.

## 2 OBSERVATIONS AND DATA ANALYSIS

We have observed RBS 1124 with *Suzaku* on 2007 April 14th (observation ID: 702114010) obtaining a net exposure of 86 ks ( $\sim 140 \text{ ks}$  total exposure). The source was placed at the HXD nominal position. Products for the three available XIS units (the two front-illuminated CCD XIS 0 and XIS 3 and the back-illuminated CCD XIS 1, hereafter FI and BI CCD) and for the HXD PIN have been extracted following the appropriate version of the *Suzaku* Data Reduction Guide<sup>1</sup>. Our analysis is based on data processing version 2.0.6.13 and is carried out with the HEASOFT 6.6.2 software and the *Suzaku* CALDB released on 2009–04–03. The XIS data have been analysed starting from the unscreened event files and by applying the XISPI tool and standard screening criteria to produce screened cleaned event files (see Chapter 6 of the *Suzaku* Data Reduction Guide). Appropriate RMF and ARF files have been generated with the XISRMFGEN and XISSIMARFGEN tools. As for the HXD/PIN, besides standard reduction, we have accounted for the Cosmic X-ray background (CXB) by simulating the CXB contribution to the PIN background according to the recipes in Chapter 7 of the *Suzaku* Data Reduction Guide. Given that the CXB model in the hard energy band still suffers from a  $\sim 10$  per cent uncertainty (Roberto Gilli, private communication), we included a 10 per cent systematic uncertainty to the CXB spectrum and we then added the corrected CXB spectrum to the instrumental non X-ray background (NXB) provided by the *Suzaku* team to which a 1.4 per cent systematic uncertainty was also added (following Fukazawa et al. 2009). We use the appropriate PIN response matrix for the epoch of the observation at the HXD nominal position.

RBS 1124 was also observed by *Swift*/XRT on four occasions from 2007–05–24 to 2007–07–21, i.e. starting about 40 days after the *Suzaku* observation (observation ID 00036542001, 00036542002, 00036542003, and 00036542004) with exposures in the range of 0.6–5.3 ks. *Swift*/BAT data were collected in survey mode and cannot be analysed in this work due to the limited public availability of the analysis software. In all observations, XRT data were accumulated in Photon Counting (PC) mode and we present here the XRT/PC data for the first time. We processed these data with the XRTPIPELINE (v.0.12.1), and we applied standard filtering and screening criteria. Source and background light curves and spectra were extracted by selecting standard event grades of 0–12, and using circular extraction regions with radii of 20 pixels. We created exposure maps by using the XRTEXPOMAP task, and used the latest spectral redistribution matrices available from the *Swift* CALDB. Ancillary response files, accounting for different extraction regions, vignetting and PSF corrections, were generated by using the XRTMKARF task. As discussed in the text, given that the

<sup>1</sup> Available at <http://heasarc.gsfc.nasa.gov/docs/suzaku/analysis/abc/>

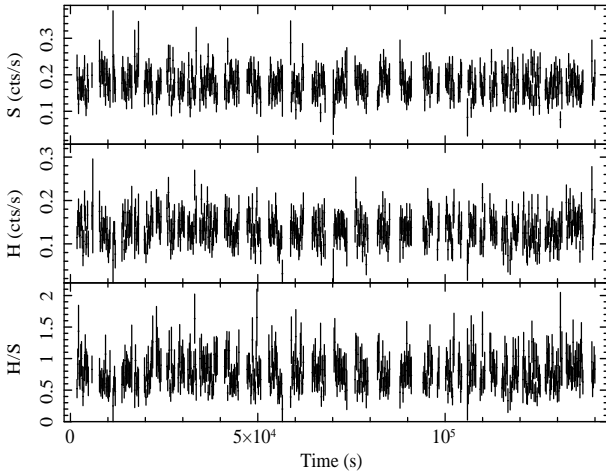


**Figure 1.** The background subtracted XIS 3 light curves with 200 s time bins. In the two top panels we show the soft (S) 0.5–2 keV and hard (H) 2–10 keV light curves, while the bottom panel displays their ratio (simply defined as H/S).

single spectra are all consistent with the same shape and X-ray flux, we have co-added the four available XRT/PC exposures to produce a single spectrum with an exposure of  $\sim 14$  ks.

Spectral analysis is performed with the XSPEC v.12.5 software. All *Suzaku* spectra are grouped to a minimum of 50 counts per bin (20 for the XRT/PC spectra) to ensure the applicability of  $\chi^2$  statistics. We report 90 per cent errors ( $\Delta\chi^2 = 2.706$  for 1 parameter) unless stated otherwise. Fluxes below 10 keV are those observed with the *Suzaku* XIS 0 detector (or with the XRT/PC, when stated). We adopt a standard  $\Lambda$ CDM cosmology with  $H_0 = 70 \text{ km s}^{-1}$ ,  $\Omega_\Lambda = 0.73$ , and  $\Omega_M = 0.27$ .

### 3 THE 2–10 KEV SPECTRUM AND FE EMISSION LINE

The 0.5–10 keV XIS 0 light curve of RBS 1124 is shown in Fig. 1 together with the hard to soft counts ratio light curve (H/S where H and S are the count rates in the 2–10 keV and 0.5–2 keV band respectively). No significant flux nor spectral variability is present throughout the exposure. We then proceed with the analysis of the time-averaged properties of the source.

We start our analysis by considering joint fits to the XIS spectra in the restricted 2–10 keV (FI) and 2–8 keV (BI) band. We first apply a simple power law model modified by photoelectric absorption fixed at  $1.5 \times 10^{20} \text{ cm}^{-2}$  (the Galactic column in the line of sight, Kaberla et al 2005). The data are well described by this simple model ( $\chi^2 = 665$  for 661 degrees of freedom, dof) and we obtain  $\Gamma = 1.70 \pm 0.05$ , and a 2–10 keV flux of  $\simeq 5.1 \times 10^{-12} \text{ erg cm}^{-2} \text{ s}^{-1}$ , corresponding to a 2–10 keV unabsorbed luminosity of  $\simeq 6.1 \times 10^{44} \text{ erg s}^{-1}$ . No striking residuals are present over the whole 2–10 keV band. However, visual inspection of the residuals may not be the most efficient way to look for spectral features. A more efficient visual representation of the residuals is given in Fig. 2 where we use the method outlined in Miniutti & Fabian (2006) and run a Gaussian emission line filter through the data varying its energy between 4 keV and 8 keV and its intensity in the  $\pm 1 \times 10^{-4} \text{ ph cm}^{-2} \text{ s}^{-1}$  range, while keeping its width fixed at 1 eV, and we record the statistical improvement. This procedure highlights that excess emission is present around 6.4 keV in

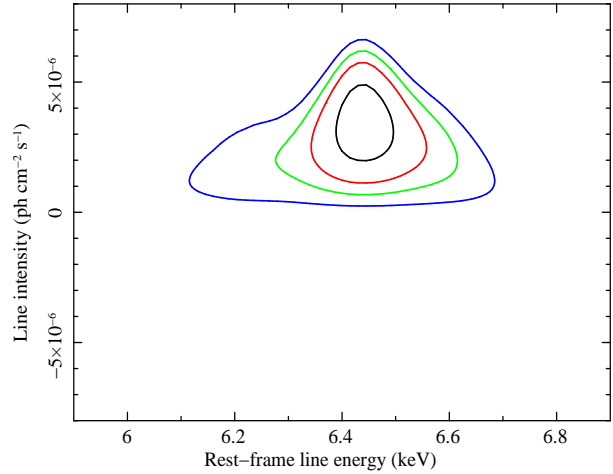


**Figure 2.**  $\Delta\chi^2$  contours when a Gaussian filter is run through the data modelled with a simple absorbed power law. No other features are present in the explored intensity–energy plane (see text), so we restrict the axis ranges in the Figure for clarity. From outermost to innermost, the contours represent  $\Delta\chi^2 = -2.28, -5.99, -9.21, -13.816$ , corresponding approximately to 68, 95, 99, and 99.9 per cent confidence regions.

the rest-frame and the contours suggest a statistical significance of more than  $3\sigma$ .

We then add a Gaussian emission line to our model with energy, width, and normalisation free to vary. We obtain a significant improvement of  $\Delta\chi^2 = -22$  for 3 dof, i.e.  $\chi^2 = 643$  for 658 dof, corresponding to a significance at the 99.9999 per cent level according to a simple F-test (used to roughly estimate the true statistical significance) and we measure a line energy of  $6.40 \pm 0.10 \text{ keV}$ , consistent with neutral Fe. The line is resolved, although not extremely broad, with  $\sigma = 0.17^{+0.10}_{-0.06} \text{ keV}$  and has an equivalent width  $EW = 60 \pm 25 \text{ eV}$ .

Since a narrow 6.4 keV Fe line is ubiquitous in the X-ray spectra of AGN (see e.g. Bianchi et al. 2007), we then consider a model comprising two Gaussian emission lines, one representing the putative narrow line with energy  $E \equiv 6.4 \text{ keV}$  and width  $\sigma \equiv 1 \text{ eV}$ , the other (with all parameters free to vary) accounting for the broader component. No improvement is however obtained with respect to the best-fitting model described above (one broadish Gaussian only), and the narrow line intensity is only an upper limit. Given that the narrow line is not detected, we remove it from our spectral model. In order to check whether the broad line width could be partially due to the presence of a Compton shoulder (e.g. Matt 2002), we include an Gaussian emission line with energy fixed at 6.3 keV and  $\sigma \equiv 40 \text{ eV}$ . However, the Compton shoulder intensity tends to zero and no change in the width of the 6.4 keV line is measured. We then conclude that the Fe emission line we observe is broad with respect to the XIS energy resolution and we remove the Compton shoulder component from our model.

If the broad line energy, width, and normalisation is allowed to vary between the three detectors, no significant changes in the line parameters are obtained for the two FI spectra, while the BI one provides consistent but less constrained results (due to the lack of sensitivity above 7–8 keV). Thus the line is marginally resolved and line parameters are consistent in the XIS detectors independently, with better constraints coming from the two FI spectra.

The detected broad line has energy consistent with neutral Fe  $K\alpha$  emission. It is thus unlikely that its width could be explained by Comptonization by partially ionized gas. Moreover, the lower

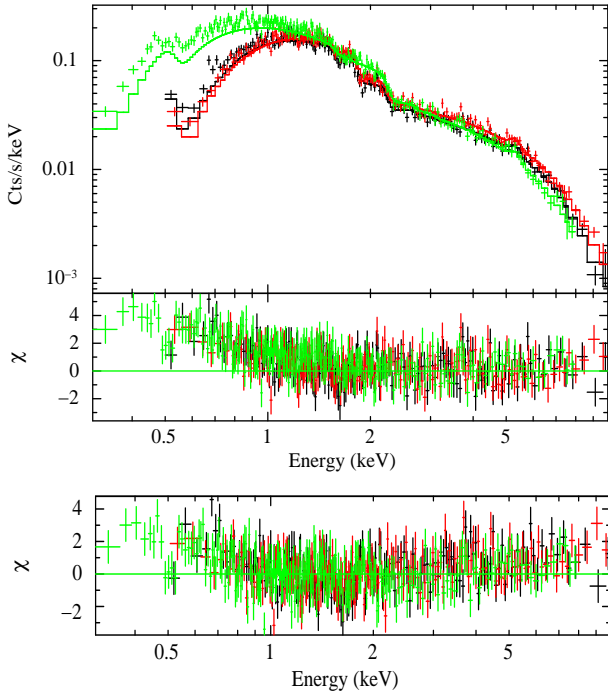


**Figure 3.** In the top panel we show the extrapolation to soft X-rays of our simple 2–10 keV power law (plus Gaussian) model which shows excess emission below  $\sim 1$ –2 keV. The BI spectrum is the one extending to softer energies (green in the on-line version), while the two FI spectra superimpose almost exactly (XIS 0 in black and XIS 3 in red in the on-line version). In the bottom panel, we show the residuals left once the data have been re-fitted with the same model. The model attempts to describe the soft excess by steepening the power law photon index, which however provides a worse description in the hard band. We conclude that the soft excess is most likely real and that the 0.3–10 keV spectral shape cannot be described by a simple power law model. The x-axis energy is in the observed frame.

limit on the line width ( $\sigma \geq 0.11$  keV) corresponds to a FWHM of  $\geq 1.2 \times 10^4$  km s $^{-1}$ , much larger than the H $\beta$  FWHM =  $4.26 \pm 1.25 \times 10^3$  km s $^{-1}$  (Grupe et al. 2004), excluding that the Fe K $\alpha$  line comes from the broad line regions and suggesting an origin in reflection off material much closer to the central black hole. The natural production site is then the accretion disc, where velocity and gravitational shifts can contribute to broaden the line profile. In this case the fluorescent line emission must be associated with a full reflection spectrum which also produces a soft excess for a wide range of ionization states (e.g. Ross & Fabian 1993; Zycki 1994; Nayakshin, Kazanas & Kallman 2000; Rozanska et al. 2002; Ross & Fabian 2005). We will consider such model after extending the energy range of our spectral analysis.

#### 4 INCLUDING THE SOFT X-RAY DATA: THE NEED FOR A MULTI-COMPONENT SPECTRAL MODEL

The extrapolation of our best-fitting model to the soft energies (down to 0.5 keV for the FI spectra and 0.3 keV for the BI), reveals a relatively weak soft excess, as shown in the top panel of Fig. 3. Re-fitting the data with the same model provides a relatively poor description of the data ( $\chi^2 = 1672$  for 1466 dof) with a steeper photon index than before ( $\Gamma = 1.85 \pm 0.04$ ). The residuals do not look satisfactory and exhibit some curvature both in the hard and soft band, suggesting that the soft excess is real and that the 0.3–

10 keV band spectrum has to be described with a multi-component model rather than with a simple power law. This is shown in the bottom panel of Fig. 3. We note that an absorption feature seems to be present around 0.5 keV ( $\sim 0.6$  keV in the rest-frame). This feature will be discussed when more appropriate spectral models will be used.

#### 5 A SELF-CONSISTENT DISC REFLECTION MODEL

Given that we have evidence for a relatively broad Fe line we first consider a two-component model comprising a power law continuum and an X-ray reflection spectrum (from Ross & Fabian 2005) which is convolved with the relativistic kernel KDBLUR to account for the spectral distortions induced by the large orbital velocity and strong gravity effects in the inner accretion disc. The relativistic blurring parameters are the same as for the LAOR XSPEC model (Laor 1991), except that the spectrum to be affected is the full X-ray reflection spectrum and not just a narrow emission line. We fix the outer disc radius at its maximum allowed value of  $400 r_g$  (where  $r_g = GM/c^2$ ), while the emissivity index  $q$  (where the emissivity is parametrised as  $\epsilon(r) \propto r^{-q}$ ), the disc to observer inclination  $i$ , and the inner disc radius  $r_{in}$  are free to vary. As for the reflection model, the photon index of the irradiating continuum and its high-energy cut-off are tied to the power law (the cut-off is fixed at 100 keV, as assumed in the Ross & Fabian reflection grid of models), the Fe abundance is fixed at the Solar value, while the ionization state of the reflector and the overall reflection normalisation are free parameters.

We obtain a very good description of the 0.3–10 keV XIS data with  $\chi^2 = 1500$  for 1464 dof reproducing well the soft excess, Fe line, and general spectral shape. In other words, the power law plus disc reflection model provides a statistical improvement of  $\Delta\chi^2 = -172$  for  $\Delta dof = -2$  in the 0.3–10 keV band with respect to the previous power law plus Gaussian model. Before discussing the relevant parameters, we note that removing the relativistic blurring kernel (i.e. fitting the data with a power law plus unblurred reflection) produces a much worse description of the data with  $\Delta\chi^2 = +40$  for  $\Delta dof = +3$ , i.e. the relativistic blurring is required at the more than the  $6\sigma$  level. Since the line model has now changed with respect to the broad Gaussian used above, we re-consider the issue of whether a narrow 6.4 keV Fe K $\alpha$  line is present by including a narrow Gaussian emission line (with  $E \equiv 6.4$  keV and  $\sigma \equiv 1$  eV) in our model. The narrow Fe line produces a further statistical improvement of  $\Delta\chi^2 = -10$  for 1 dof, i.e. the narrow line is now detected at more than the  $3\sigma$  level with an equivalent width of  $25 \pm 13$  eV. The narrow line component was not required when using the previous Gaussian model, which is understandable giving that the broad line is now asymmetric, skewed towards low energies, and peaks at slightly higher energy than 6.4 keV thus leaving some room for a narrower line component (see e.g. the top panel of Fig. 5). A further absorption feature is seen in the residuals (see also Fig. 3) and can be modelled with a narrow ( $\sigma \equiv 1$  eV) Gaussian absorption line at  $E_{abs} \simeq 0.61$  keV. Despite its low equivalent width ( $EW_{abs} \simeq -8$  eV) and a somewhat uncertain identification (no strong absorption feature is expected at 0.61 keV) we include it in our model since it provides a statistical improvement ( $\Delta\chi^2 = -10$  for 2 dof for a final result of  $\chi^2 = 1480$  for 1461 dof) but we cannot exclude that it has an instrumental origin.

Our best-fitting model results in a 2–10 keV observed flux of  $\simeq 5.1 \times 10^{-12}$  erg cm $^{-2}$  s $^{-1}$ , while the 2–10 keV unabsorbed lu-

**Table 1.** Best-fitting parameters for the power law plus relativistically blurred reflection model, also comprising an additional narrow Fe K $\alpha$  line with intensity  $I_{\text{NL}}$  and equivalent width  $EW_{\text{NL}}$  and a soft absorption line with energy  $E_{\text{abs}}$  and equivalent width  $EW_{\text{abs}}$ . The superscript  $f$  denotes that the high-energy cut-off parameter is fixed at 100 keV.

$\Gamma$	$1.85 \pm 0.08$
$E_c$ [keV]	$100^f$
$i$ [degrees]	$33 \pm 6$
$q$	$4.1^{+5.3}_{-0.9}$
$r_{\text{in}}$ [ $r_g$ ]	$\leq 3.2$
$\xi_{\text{ref}}$ [erg cm s $^{-1}$ ]	$40^{+70}_{-30}$
$I_{\text{NL}}$ [ph cm $^{-2}$ s $^{-1}$ ]	$(2.8 \pm 1.4) \times 10^{-6}$
$EW_{\text{NL}}$ [eV]	$25 \pm 13$
$E_{\text{abs}}$ [keV]	$0.61 \pm 0.05$
$EW_{\text{abs}}$ [eV]	$-8 \pm 6$
$F_{2-10 \text{ keV}}$ [erg cm $^{-2}$ s $^{-1}$ ]	$\simeq 5.1 \times 10^{-12}$
$L_{2-10 \text{ keV}}$ [erg s $^{-1}$ ]	$\simeq 6.0 \times 10^{44}$
$\chi^2/\text{dof}$	1480/1461

minosity is  $\simeq 6.0 \times 10^{44}$  erg s $^{-1}$ . In order to compute the source bolometric luminosity from the 2–10 keV one, we adopt a bolometric correction of 50 (e.g. Marconi et al. 2004) which however refers to the intrinsic 2–10 keV luminosity (i.e. the power law luminosity  $\sim 4.8 \times 10^{44}$  erg s $^{-1}$ ) leading to  $L_{\text{Bol}} \simeq 2.3 \times 10^{46}$  erg s $^{-1}$ . Assuming a black hole mass of  $1.8 \times 10^8 M_{\odot}$ , RBS 1124 turns out to be particularly radiatively efficient with an estimated Eddington ratio of  $\sim 1$ .

As for the most relevant best-fitting parameters, the ionization state is constrained to be  $\xi = 40^{+70}_{-30}$  erg cm s $^{-1}$  in which range the dominant Fe line is the K $\alpha$  at 6.4 keV, in agreement with our previous findings. We measure a photon index of  $\Gamma \simeq 1.85$ , steeper than the power law model fitted in the 2–10 keV band because the model now also comprises the X-ray reflection spectrum, which is very hard in the 2–10 keV band (equivalent  $\Gamma \simeq -0.1$ ). The relativistic blurring best-fitting parameters are  $i = 33^\circ \pm 6^\circ$ ,  $q = 4.1^{+5.3}_{-0.9}$ , and  $r_{\text{in}} \leq 3.2 r_g$ . We note that the emissivity index is basically unconstrained and our result translates effectively into  $q \geq 3.2$  at the 90 per cent level. A summary of the inferred best-fitting parameters for the final model is given in Table 1.

Our result on the inner disc radius ( $r_{\text{in}} \leq 3.2 r_g$ ) is particularly intriguing. Under the standard assumption that the inner disc radius coincides with the innermost stable circular orbit (ISCO) of the black hole spacetime,  $r_{\text{in}}$  only depends on black hole spin (with larger ISCO corresponding to smaller spin, Bardeen, Press & Teukolsky 1972). The upper limit we measure translates into a lower limit of  $a \geq 0.74$  for the black hole spin, suggesting that the black hole in RBS 1124 is a rapidly rotating Kerr one. To investigate in some more detail this important result, and to check upon the possibility that it may be driven by a local rather than global  $\chi^2$  minimum, we have considered contour plots on the two most relevant parameters, namely the inner disc radius and the emissivity index. We consider these two parameters because they can in principle be degenerate since both small inner radii and steep emissivity profiles tend to produce broader and more redshifted line shapes, while the disc inclination has a more independent effect, especially for the intermediate  $\simeq 33^\circ$  value we measure. The result of this exercise is shown in Fig. 4. As already suggested by errors on single parameters, the emissivity index is basically only constrained to be  $q \geq 3$ , but for any allowed value of  $q$ ,  $r_{\text{in}}$  never exceeds a rather

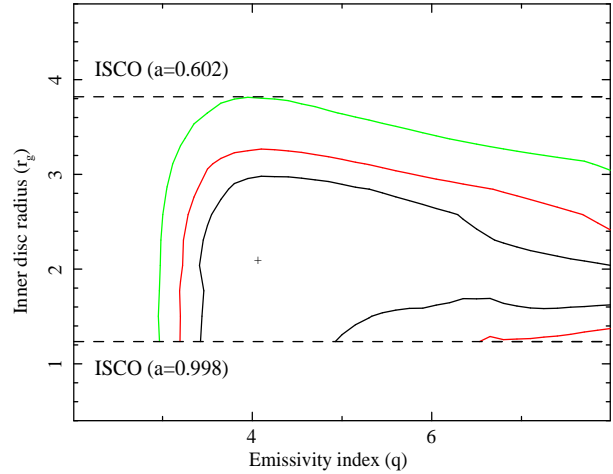


**Figure 4.**  $\Delta\chi^2 = 2.3, 4.61, 9.21$  contours (corresponding to approximate 68.3, 90, and 99 per cent confidence regions) for the two most relevant relativistic parameters, namely the inner disc radius and the emissivity index. The two horizontal lines mark the ISCO and the associated black hole spin value. Under the assumption that the disc extends down to the ISCO, the black hole spin is constrained to be  $a \geq 0.60$  at the 99 per cent level for two significant parameters.

small limiting radius. We conclude that  $r_{\text{in}} \leq 3.8 r_g$  at the 99 per cent level, which translates into a spin  $a \geq 0.60$ , still strongly pointing to a rapidly rotating Kerr black hole solution (see however the discussion in the following Section).

As a final remark, we point out that the reflection model we use does not allow to compute the reflection fraction  $R$  directly. However, it can be approximately estimated using the relationship in Brenneman et al. 2009 (see their Eq. 1) which, in our case, gives  $R \sim 0.6$ . Note that the inferred reflection fraction is broadly consistent with the relatively small measured broad plus narrow Fe line equivalent width ( $\simeq 85$  eV) for solar Fe abundance (George & Fabian 1991). This amount of reflection should be partly associated with the broad line ( $R_{\text{disc}}$ ) and partly with the narrow Fe line (most likely originating in reflection off distant material such as the obscuring torus,  $R_{\text{torus}}$ ). The splitting between these two components can be roughly estimated by comparing the lines EW, i.e.  $EW_{\text{broad}}/EW_{\text{narrow}} \simeq R_{\text{disc}}/R_{\text{torus}} \simeq 2.4$  and thus  $R_{\text{disc}} \simeq 0.42$  and  $R_{\text{torus}} \simeq 0.18$ .

### 5.1 On the reliability of the inferred $r_{\text{in}}$ (and black hole spin)

We must point out that our result on  $r_{\text{in}}$  is somewhat surprising. According to the Fe line shape (see e.g. Fig. 2) and Gaussian width ( $\sigma \simeq 0.17$ ), the red wing of the line is not extended to very low energies. It is difficult then to claim that the Fe line shape implies  $r_{\text{in}} \leq 3.8$  because such a small inner radius should result in a much more extended red wing (see e.g. Fabian & Miniutti 2009). The small reflection fraction we measure implies that only the relatively narrow blue peak of the broad Fe line is observable above the continuum, which is consistent with the relatively small  $\sigma$  we infer for the line, but it is clear that the breadth of the Fe line red wing that is detectable above the continuum is not extended enough to imply such a small inner disc radius. A possible explanation for this apparent discrepancy is that  $r_{\text{in}}$  is primarily driven by the need to describe a smooth soft excess with the disc reflection model. Large  $r_{\text{in}}$  cannot be able to account for a smooth soft excess because the

reflection soft X-ray lines (e.g. Oxygen, Fe L, and others) would not be sufficiently blurred.

To test whether the smaller inner disc radius is driven by the soft excess smoothness we restrict the fitting interval to the 2–10 keV band. We obtain a good representation of the data with  $\chi^2 = 640$  for 655 dof. As for the most relevant parameter, we measure a much larger inner disc radius of  $r_{\text{in}} \simeq 100 r_g$  (but basically unconstrained). We thus conclude, as already suspected, that the Fe line profile alone does not require the presence a disc with small  $r_{\text{in}}$ . It is only when the soft X-ray data are considered, and under the assumption that the soft excess is due to disc reflection, that a small inner disc radius is required by the data. The main blurring parameters are then driven by the soft X-ray excess smoothness and the Fe line only sets the overall reflection normalisation and strength with respect to the continuum. Consistency between the soft and Fe line data is achieved with a small inner disc radius and a small reflection fraction, but the inferred  $r_{\text{in}}$  (and thus black hole spin  $a$ ) is not driven by the Fe line shape. Hence, the derived black hole spin lower limit ( $a \geq 0.60$ ) is in this case particularly interpretation-dependent and relies on the idea that the soft excess is due to X-ray reflection from the accretion disc. As mentioned before, the reflection fraction is lower than standard, and this explains why the red wing of the broad line is buried in the continuum, while only the relatively narrow blue peak of the line is confidently detected above the continuum level.

The idea that the soft X-ray excess in AGN is due to disc reflection is well motivated physically and is generally very successful when tested on X-ray data (see e.g. Fabian et al. 2004; Ponti et al. 2006; Miniutti et al. 2009b; Fabian et al. 2009), but it is nonetheless a non unique interpretation. It should be however pointed out that the detection of a short  $\sim 30$  s lag between the continuum and the soft excess in the Narrow-Line Seyfert 1 galaxy 1H 0707–495 points towards the idea that the soft excess is indeed part of a reprocessed component, favouring the reflection interpretation in this extreme source (Fabian et al. 2009). We also point out here that the high Eddington ratio we infer from the X-ray luminosity suggests very strongly that a radiatively efficient inner disc/corona structure is present, unless the black hole mass estimate of RBS 1124 (or the used bolometric correction) is wrong by at least one order of magnitude, which seems unlikely. Hence the question is not, in our opinion, whether the accretion flow extends down to/near the ISCO, but rather whether we can constrain its inner radius and the spacetime geometry precisely through X-ray data analysis in this particular QSO.

## 6 A PARTIAL-COVERING ALTERNATIVE

We have seen above that, under the assumption that the broadband spectrum is shaped by a standard X-ray power law continuum plus its reflection from the disc, a disc extending down to the ISCO of a rapidly rotating Kerr black hole is required by the data. However, as mentioned above, our result depends strongly on the assumption that the soft X-ray excess is due to disc reflection.

We consider here, as a possible alternative to the reflection model presented above, a scenario in which the 0.3–10 keV spectrum of RBS 1124 is described by a simple power law seen however through a column of partially ionized gas which covers only partially the X-ray emitting region. Our model comprises Galactic absorption, a power law, a Gaussian emission line (with energy, width, and normalisation free to vary), and a partially ionized partial covering model (the ZXIPCF model in XSPEC) characterised by

**Table 2.** Best-fitting parameters for the partial covering model (with covering fraction  $Cf$ ), also comprising a resolved Fe emission line and the soft absorption line already present in the reflection model (see Table 1).

$\Gamma$	$2.01 \pm 0.07$
$N_{\text{H}}$ [ $\text{cm}^{-2}$ ]	$6.0^{+3.0}_{-2.0} \times 10^{22}$
$\log \xi$	$-0.5^{+0.7}_{-2.5}$
$Cf$	$0.36 \pm 0.07$
$E_{\text{Fe}}$ [keV]	$6.40 \pm 0.10$
$\sigma_{\text{Fe}}$ [keV]	$0.16^{+0.14}_{-0.06}$
$I_{\text{Fe}}$ [ $\text{ph cm}^{-2} \text{s}^{-1}$ ]	$(5.7 \pm 2.7) \times 10^{-6}$
$EW_{\text{Fe}}$ [eV]	$58 \pm 30$
$E_{\text{abs}}$ [keV]	$0.61 \pm 0.06$
$EW_{\text{abs}}$ [eV]	$-8 \pm 6$
$L_{2-10 \text{ keV}}$ [ $\text{erg s}^{-1}$ ]	$\simeq 7.3 \times 10^{44}$
$\chi^2/\text{dof}$	1482/1461

three free parameters (column density, ionization state, and covering fraction). We apply the model to the 0.3–10 keV XIS data and we obtain a very good description of the spectral shape, statistically equivalent to the one discussed above ( $\chi^2 = 1493$  for 1463 dof). As in the previous model, adding a soft absorption line at  $\sim 0.61$  keV improves the fit to  $\chi^2 = 1482$  for 1461 dof, a result which cannot be statistically distinguished from the reflection-based one ( $\chi^2 = 1480$  for the same number of dof). A summary of the best-fitting model parameters is given in Table 2.

The partial coverer has a column density  $N_{\text{H}} = 6.0^{+3.0}_{-2.0} \times 10^{22} \text{ cm}^{-2}$ , ionization parameter  $\log \xi = -0.5^{+0.7}_{-2.5}$ , and covers  $36 \pm 7$  per cent of the X-ray emitting region, while the intrinsic spectral shape is characterised by  $\Gamma = 2.01 \pm 0.07$ . As for the Gaussian emission line, we measure  $E = 6.4 \pm 0.1$  keV,  $\sigma = 0.16^{+0.14}_{-0.06}$  keV for a line EW of  $58 \pm 30$  eV. In the partial covering scenario, the unabsorbed 2–10 keV luminosity is  $\sim 7.3 \times 10^{44} \text{ erg s}^{-1}$  which implies an Eddington ratio of  $\sim 1.5$ , significantly higher than that estimated with the previous reflection model ( $\sim 1$ ). Again, such high Eddington ratio tells us that radiatively efficient accretion is taking place even when a partial covering scenario is considered, so that a disc/corona structure close to the ISCO is most likely present. The question is whether the inner accretion flow is visible (e.g. through X-ray reflection) or masked by absorption.

The absorber ionization parameter is low and no strong absorption lines are predicted by the model so that no velocity shifts can be measured. The low ionization state is consistent with the idea that the neutral Fe  $K\alpha$  line we detect originates from reflection and/or transmission in the gas responsible for the partial covering. If the observed Fe line can be produced by the absorber, the model would have the same satisfactory level of self-consistency than the reflection model presented above with only two components (continuum and either disc reflection or partial covering absorption) accounting for the whole 0.3–10 keV spectral shape. We first check the significance of the resolved width of the Fe line by forcing it to be unresolved ( $\sigma \equiv 1$  eV) and by refitting the data. This procedure provides a  $\Delta\chi^2 = +6.4$  with respect to the case of a broad line, i.e. the Fe line is resolved at the 98.8 per cent level according to the F-test.

Assuming that the Fe line is associated with the absorber, its FWHM can be used to constrain the absorber location  $R_{\text{abs}}$  under the hypothesis that the absorbing gas moves with isotropic Keplerian velocity  $v_{\text{abs}} = \sqrt{3}/2$  FWHM. On the other hand, the ion-



ization state of the absorber is defined in the ZXIPCF model as  $\xi = L \Delta R_{\text{abs}} N_{\text{H}}^{-1} R_{\text{abs}}^{-2}$  (where  $L$  is the central engine luminosity<sup>2</sup> and  $\Delta R_{\text{abs}}$  is the absorber thickness) and can thus be used to constrain the absorber relative thickness  $\Delta R/R = \xi R_{\text{abs}} N_{\text{H}}/L$ . By using the available upper values of  $\xi$ ,  $R_{\text{abs}}$ ,  $N_{\text{H}}$  and lower value of the intrinsic luminosity, we estimate  $\Delta R/R \leq 6 \times 10^{-6}$  for a black hole mass of  $1.8 \times 10^8 M_{\odot}$ . The inferred  $\Delta R/R$  is implausibly small, indicating that our basic assumption, namely that the Fe line is produced by the absorber, is not correct. We are thus left with an unknown origin for the Fe line we observe, so that the partial covering scenario is less self-consistent than the reflection one and does require an additional emission component to account for the resolved Fe  $K\alpha$  emission line. Moreover, since the Fe line is resolved, the additional component cannot be the standard obscuring torus of AGN unification schemes because such material is located at the  $\sim \text{pc}$  scale, thus producing unresolved emission lines.

## 7 THE BROADBAND 0.3–30 KEV SPECTRUM

The two competing models presented above (disc reflection and partial covering) make somewhat different predictions above 10 keV. We then consider the HXD/PIN data in the 14–30 keV range where the source is detected with good statistics. The PIN signal in that band is about 8.8 per cent of the combined non X-ray and Cosmic X-ray backgrounds (NXB and CXB). We introduce a cross-normalisation PIN/XIS 0 constant of  $1.18 \pm 0.02$  as discussed in Maeda et al (2008<sup>3</sup>). Plain extrapolation of the 0.3–10 keV best-fitting models gives  $\chi^2 = 1539$  and  $\chi^2 = 1603$  for the reflection and partial covering models respectively for the same number of dof (1502). Refitting the data does not improve much the reflection model statistics ( $\chi^2 = 1535$ ) and we do not observe any significant changes in the parameters, while a more substantial improvement is obtained in the partial covering case ( $\chi^2 = 1562$ ) resulting in a covering fraction of  $\sim 55$  per cent with much larger  $N_{\text{H}} = (1.2 \pm 0.2) \times 10^{24} \text{ cm}^{-2}$  and  $\log \xi = 2.3 \pm 0.3$ . Note however that in this case the intrinsic 2–10 keV luminosity becomes  $\simeq 1.1 \times 10^{45} \text{ erg s}^{-1}$ , corresponding to a perhaps implausibly high super-Eddington ratio of  $\simeq 2.4$ . In Fig. 5 we show the best-fitting reflection model (top panel), the data, model, and residuals for the reflection model (middle panel), and the residuals for the best-fitting partial covering one (bottom panel).

It should be stressed that, even for the best-fitting reflection model, the 14–30 keV PIN data are underestimated (see bottom panel of Fig. 5). By assuming a  $\Gamma \equiv 2$  power law fitted only to the PIN data, we measure an excess flux of  $\simeq 2 \times 10^{-12} \text{ erg cm}^{-2} \text{ s}^{-1}$  at the 99.1 per cent confidence level according to the F-test. We have inspected the quasi-simultaneous *Swift* XRT/PC images (see Section 8 below) to look for possible contaminating hard X-ray sources, but we only detected two sources above 3 keV in a  $9 \times 9$  arcmin region around RBS 1124 and they have a cumulative extrapolated 14–30 keV flux (assuming  $\Gamma \equiv 2$ ) of  $\simeq 2.5 \times 10^{-13} \text{ erg cm}^{-2} \text{ s}^{-1}$ , i.e. about one order of magnitude below the observed excess. The PIN field of view is larger (about  $34 \times 34$  arcmin), but an archive-based search did not provide any X-ray source that could explain the observed PIN excess.

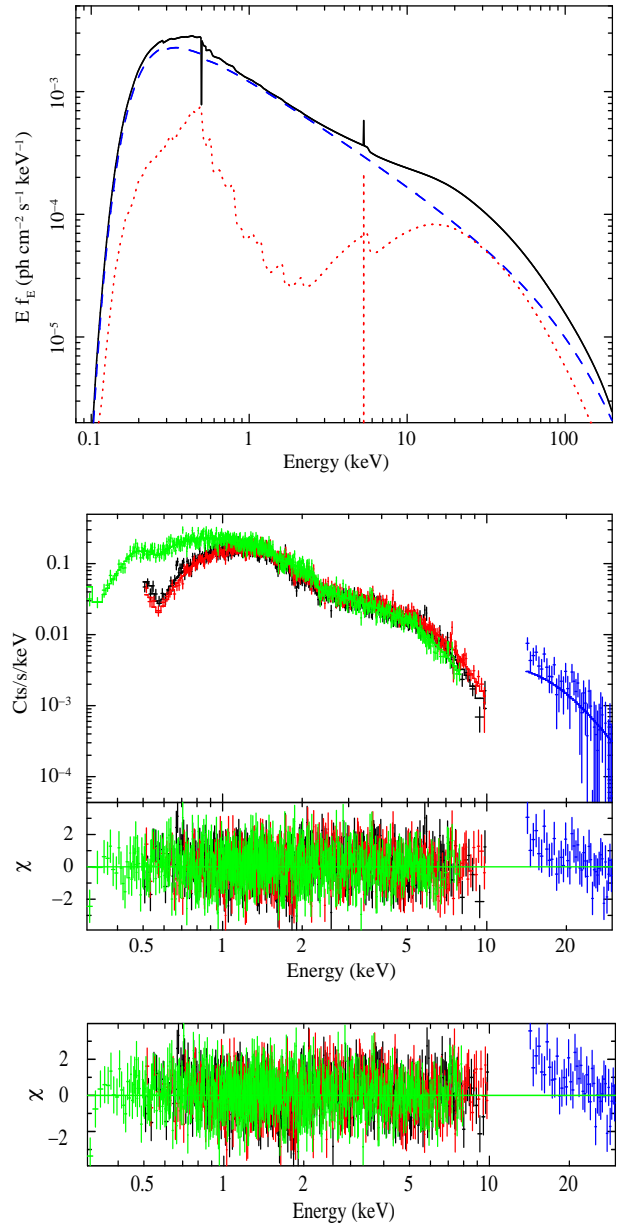


**Figure 5.** In the top panel we show the best-fitting two-component model (power law plus disc reflection) including also the unresolved narrow Fe  $K\alpha$  emission line at 6.4 keV and the  $\sim 0.61$  keV absorption line. In the middle panel, we show XIS and PIN data, best-fitting reflection model, and residuals. In the bottom panel, we show the residuals for the best-fitting partial covering model. The same detector color scheme as in Fig. 3 is used, and the PIN data are shown in blue in the on-line version. Note the weak excess in the PIN 14–30 keV band for both adopted models (see text for discussion). The x-axis is in the observed frame.

We cannot exclude that a variable hard X-ray source is contaminating the PIN data and therefore we do not attach to much significance to the better statistical result obtained with the reflection model when fitting the PIN data. However, as mentioned, the best-fitting partial covering model in the 0.3–30 keV band would require that RBS 1124 is radiating at a super-Eddington rate, which seems unlikely.

<sup>2</sup> In the partial covering model we use the intrinsic luminosity  $L$ , defined as the continuum luminosity in the 1–1000 Ry range. We estimate  $L$  by extrapolating our unabsorbed power law continuum model in that range.

<sup>3</sup> JX-ISAS-SUZAKU-MEMO-2008-06.

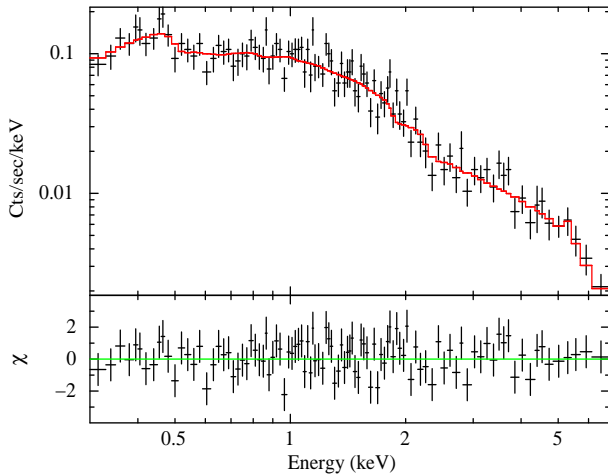


**Figure 6.** The co-added *Swift* XRT/PC spectrum (14 ks of total exposure) together with the best-fitting reflection model and residuals. An identical statistical quality is reached when the partial covering model is used instead.

## 8 LONG-TERM SPECTRAL VARIABILITY

As mentioned, RBS 1124 was detected in the RASS on 1990–10–26 and by the *XMM-Newton* Slew Survey on 2006–11–25. In 2007, it was also observed 4 times by *Swift* from May 24 to July 21 and data from the XRT/PC are available.

The RASS spectrum is well represented by a simple  $\Gamma \simeq 2.38$  power law, affected by Galactic absorption resulting in a 0.2–2 keV flux of  $7.6 \times 10^{-12}$  erg cm $^{-2}$  s $^{-1}$  (Grupe et al. 2001). By assuming the same spectral shape, the *XMM-Newton* Slew Survey flux is  $6.5 \times 10^{-12}$  erg cm $^{-2}$  s $^{-1}$  in the same band, implying limited flux variability in the two observations separated by  $\sim 16$  years. For comparison, a similar fit to the *Suzaku* data (taken on 2007–04–14) yields a slightly harder slope  $\Gamma = 1.95 \pm 0.03$  and a much smaller 0.2–2 keV flux of  $(4.07 \pm 0.07) \times 10^{-12}$  erg cm $^{-2}$  s $^{-1}$ . We conclude that RBS 1124 was at its brightest during the RASS and has now dropped in flux by slightly less than 50 per cent with some evidence for associate hardening of the soft X-ray spectrum (from  $\Gamma_{\text{RASS}} = 2.38 \pm 0.08$  to  $\Gamma_{\text{Suzaku}} = 1.95 \pm 0.03$ ).

The *Swift* data are much closer in time to the *Suzaku* ones (a few months separation) than the RASS. We first consider the four XRT/PC spectra separately and apply a simple absorbed power law model. This results in consistent spectral slope ( $\Gamma \simeq 1.9$ ) and 0.3–10 keV flux ( $\simeq 8.2 \times 10^{-12}$  erg cm $^{-2}$  s $^{-1}$ ) in all pointings. We thus produce a co-added spectrum of all the XRT/PC observations resulting in a total exposure of  $\sim 14$  ks. Fitting the data in the 0.3–2 keV band provides  $\Gamma = 1.9 \pm 0.1$  and an extrapolated 0.2–2 keV flux of  $(4.3 \pm 0.2) \times 10^{-12}$  erg cm $^{-2}$  s $^{-1}$ , broadly consistent with the *Suzaku* results in the same band.

The XRT/PC data do not have enough quality to constrain the best-fitting models any better than *Suzaku*, but we nevertheless apply our best-fitting *Suzaku* models to the XRT/PC data to check for consistency. Both the reflection and partial covering models provide a good statistical description of the data with  $\chi^2 = 100$  for 93 dof, and no significant change in the best-fitting parameters is observed in either model with respect to the results in Table 1 and 2. In Fig. 6 we show the co-added XRT/PC spectrum together with the best-fitting reflection model and residuals.

## 9 DISCUSSION

The 0.3–10 keV X-ray spectrum of RBS 1124 can be described by i) a two-component model comprising a power law continuum and its reflection off the accretion disc, or by ii) a partial covering model in which an additional emission component is required to account for the detected resolved Fe line (we note however that the line is resolved at the 98.8 per cent confidence level). The two competing models are statistically equivalent, but the reflection model appears to be more self-consistent because it can explain all spectral features (namely the general spectral shape, the soft excess, and the Fe line) simultaneously. Moreover, when the models are applied to the 14–30 keV PIN data as well, the reflection model provides a much better statistical description of the data and, most importantly, the best-fitting partial covering one would imply a perhaps implausibly high Eddington ratio of  $\simeq 2.4$  (but see Section 7 for the uncertainties associated with the PIN data).

On the other hand, the presence of material potentially able to partially cover the X-ray source in the inner regions of accreting supermassive black holes is well established in a few cases. The most convincing cases are perhaps those in which absorber variability has been observed on relatively short timescales (e.g. Lamer, Uttley & McHardy 2003; Risaliti et al. 2009; Bianchi et al. 2009; see also Turner & Miller 2009 and references therein for a review on this active research topic). In most of the cases, the absorber variability properties point to an identification of the absorber with broad line region clouds or with disc winds originating from a similar location. As discussed above, we cannot exclude that partial covering from (for instance) broad line region clouds is occurring in RBS 1124, but the observed Fe line must come from a distinct region, closer to the central black hole, so that we need additional components in the partial covering scenario, while the reflection model is more self-consistent.

In the following we discuss the reflection scenario as the most plausible description of the X-ray properties of RBS 1124 because of its greater degree of self-consistency and because it does not invoke any additional physical component with respect to the simplest possible scenario only comprising an accretion disc and an X-ray emitting corona above it.

The most important result of our reflection-based analysis is that the inner disc radius of the reflector (disc) is tightly constrained to be  $r_{\text{in}} \leq 3.8 r_g$  at the 99 per cent level. As discussed above, this result is not driven by the relativistic Fe line shape, but rather by the soft excess smoothness which requires a high degree of relativistic blurring to mask the otherwise sharp soft X-ray emission lines reflected off the disc. Our results must then be considered as model-dependent or, better, as interpretation-dependent because it relies on the idea that soft excesses are associated with the soft part of a partially ionized reflection spectrum from the accretion disc. If our interpretation is correct, the upper limit on  $r_{\text{in}}$  translates into a lower limit for the black hole spin of  $a \geq 0.60$ , strongly suggesting that the black hole powering RBS 1124 is spinning rapidly. A small inner disc radius is also consistent with the high Eddington ratio ( $\sim 1$ ) we obtain by applying standard bolometric corrections to the 2–10 keV intrinsic luminosity. It would be very surprising if a black hole radiating away its Eddington luminosity would not possess a disc/corona structure extending down close to the black hole event horizon. The relatively high lower limit on the black hole spin may indicate that black hole growth in this object does not occur through chaotic accretion episodes (and mergers) and favours instead coherent accretion scenarios or recent mergers, as discussed in detail e.g. in Berti & Volonteri (2008).



RBS 1124 is a moderate redshift radio-quiet optically luminous quasar whose X-ray properties can be compared with the well known class of PG quasars. When a simple power law model is used, RBS 1124 hard 2–10 keV X-ray slope of  $\Gamma_h = 1.70 \pm 0.05$  is broadly consistent with the typical hard slope of PG quasars ( $< \Gamma_h > \simeq 1.87$  with a dispersion  $\sigma \simeq 0.36$ ; Piconcelli et al. 2005). On the other hand, if a simple power law model is applied in the soft band, RBS 1124 soft 0.5–2 keV X-ray spectral slope is  $\Gamma_s = 1.95 \pm 0.03$ , significantly harder than the average PG quasars value ( $< \Gamma_s > \simeq 2.73$  with a dispersion  $\sigma \simeq 0.28$ ). This indicates a relatively small soft excess in RBS 1124 with respect to the average PG quasar. In fact, if a phenomenological blackbody (BB) plus power law (PL) model is applied in the 0.3–10 keV Suzaku band, the ratio of the BB luminosity to the total one in the 0.5–2 keV band is of  $\sim 15$  per cent, about half of that typically observed (see e.g. Miniutti et al. 2009a).

In the framework of our two-component model, the soft excess strength is determined by the disc reflection ionization state and, most importantly, by the relative intensity of the reflection component with respect to the direct power law continuum (i.e. the reflection fraction). In the case of RBS 1124, the inferred disc reflection fraction is small ( $R_{\text{disc}} \sim 0.42$ ) and explains why the soft excess in this source is smaller than typical (in the standard case the disc is assumed to cover half of the sky as seen by the primary X-ray source, corresponding to  $R_{\text{disc}} \sim 1$ ). The reflector could subtend a smaller area if the disc was truncated at large radii, but this picture is not consistent with i) the measured value of  $r_{\text{in}}$  and, perhaps more importantly, ii) the high Eddington ratio of RBS 1124 and its radiatively efficient nature. In fact, truncated disc are only invoked in low-luminosity and/or radio-loud AGN and in Galactic black holes in the hard state, i.e. when the flow radiative output is highly sub-Eddington ( $L/L_{\text{Edd}} \leq 0.02$  or so).

Alternatively, the X-ray corona, which provides the hard X-ray photons irradiating the reflector, might be outflowing with mildly relativistic velocity, as suggested by Beloborodov (1999) to explain the low reflection fraction observed in Galactic black holes in the hard state. An outflow velocity of the order of  $0.25 c$  would reduce  $R$  from  $\sim 1$  to  $\sim 0.4$  due to aberration. Since RBS 1124 is radio-quiet, the corona is unlikely to be the base of a mature relativistic jet, but could possibly be associated with a failed jet. Note also that, under the assumption that the X-ray continuum is due to Comptonization and for  $\beta = v/c = 0.25$  corresponding to a Lorentz factor  $\gamma = (1 - \beta^2)^{-1/2} = 1.033$ , the Beloborodov model predicts a photon index  $\Gamma \simeq 2[\gamma(1 + \beta)]^{-0.3} \simeq 1.85$  in excellent agreement with the best-fitting value in the reflection model case ( $\Gamma = 1.85 \pm 0.08$  see Table 1). Moreover, assuming vertical motion with  $\beta = 0.25$ , mild beaming of the X-ray emission would also reduce the intrinsic 2–10 keV luminosity by a factor  $D^3 = [\gamma(1 - \beta \cos i)]^{-3} \simeq 0.53$  (where  $i$  the observer-velocity inclination) leading to  $L_{\text{Bol}} \simeq 1.2 \times 10^{46} \text{ erg s}^{-1}$  and to a reduced Eddington ratio of  $\simeq 0.5$ . Note that partial covering does not suggest beaming of the X-ray emission so that the estimated bolometric luminosity in this case is much less consistent with the literature data, predicting an Eddington ratio of 1.5 or 2.4 depending on the adopted best-fitting model in the 0.3–10 keV or 0.3–30 keV band. This further supports our interpretation of the X-ray properties of RBS 1124 in terms of reflection from the inner accretion disc of a mildly beamed X-ray continuum.

## ACKNOWLEDGEMENTS

This research has made use of data obtained from the *Suzaku* satellite, a collaborative mission between the space agencies of Japan (JAXA) and the USA (NASA). GM thanks the Ministerio de Ciencia e Innovación and CSIC for support through a Ramón y Cajal contract. CV and SB thank the Italian Space Agency (ASI) for support through grants ASI-INAF I/023/05/0 and ASI I/088/06/0. We also thank Roberto Gilli for useful discussion on the uncertainty of the CXB flux in the hard X-ray band.

## REFERENCES

- Bardeen J. M., Press W. H., Teukolsky S. A. 1972, *ApJ*, 178, 347
- Beloborodov A. M. 1999, *ApJ Letters*, 510, L123
- Berti E., Volonteri M. 2008, *ApJ*, 684, 822
- Bianchi S., Guainazzi M., Matt G., Fonseca Bonilla N. 2007, *A&A*, 467, L19
- Bianchi S., Piconcelli E., Chiaberge M., Bailón E. J., Matt G., Fiore F. 2009, *ApJ*, 695, 781
- Blustin A. J., Page M. J., Fuerst S. V., Branduardi-Raymont G., Ashton C. E. 2005, *A&A*, 431, 111
- Brenneman L. W., et al. 2009, *ApJ*, 698, 528
- Crummey J., Fabian A. C., Gallo L., Ross R. R. 2006, *MNRAS*, 365, 1067
- Czerny B., Nikolajuk M., Róžańska A., Dumont A.-M., Loska Z., Zycki P. T. 2003, *A&A*, 412, 317
- Elvis M. et al., 1994, *ApJS*, 95, 1
- Fabian A. C., Miniutti G., Gallo L., Boller T., Tanaka Y., Vaughan S., Ross R. R. 2004, *MNRAS*, 353, 1071
- Fabian A. C., Miniutti G. 2009, in “The Kerr Spacetime: Rotating Black Holes in General Relativity”, eds. D.L. Wilshire, M. Visser, S.M. Scott, Cambridge University Press (arXiv:astro-ph/0507409)
- Fabian A. C., et al. 2009, *Nature*, 459, 540
- Fukazawa Y. et al. 2009, *PASJ*, 61, 17
- George I. M., Fabian A. C. 1991, *MNRAS*, 249, 352
- Gierliński M., Done C. 2004, *MNRAS*, 349, L7
- Grupe D., Thomas H.-C., Beuermann K. 2001, *A&A*, 367, 470
- Grupe D., Wills B. J., Leighly K. M., Meusinger H. 2004, *AJ*, 127, 156
- Kalberla P. M. W., Burton W. B., Hartmann D., Arnal E. M., Bajaja E., Morras R., Pöppel W. G. L. 2005, *A&A*, 440, 775
- Lamer G., Uttley P., McHardy I. M. 2003, *MNRAS*, 342, L41
- Laor A. 1991, *ApJ*, 376, 90
- Marconi A., Risaliti G., Gilli R., Hunt L. K., Maiolino R., Salvati M. 2004, *MNRAS*, 351, 169
- Matt, G. 2002, *MNRAS*, 337, 147
- Middleton M., Done C., Gierliński M. 2007, *MNRAS*, 381, 1426
- Miniutti G., Fabian A. C. 2006, *MNRAS*, 366, 115
- Miniutti G., Ponti G., Greene J. E., Ho L. C., Fabian A. C., Iwasawa K. 2009a, *MNRAS*, 394, 443
- Miniutti G., Panessa, F., De Rosa, A., Fabian, A. C., Malizia, A., Molina, M., Miller, J. M., Vaughan, S. 2009b, arXiv:0905.2891
- Nandra K., O’Neill P. M., George I. M., Reeves J. N. 2007, *MNRAS*, 382, 194
- Nayakshin S., Kazanas D., Kallman T. R. 2000, *ApJ*, 537, 833
- Piconcelli E., Jimenez-Bailón E., Guainazzi M., Schartel N., Rodríguez-Pascual P. M., Santos-Lleó M. 2005, *A&A*, 432, 15
- Ponti G., Miniutti G., Cappi M., Maraschi L., Fabian A. C., Iwasawa K. 2006, *MNRAS*, 368, 903

- Pounds K. A., Stanger V. J., Turner T. J., King A. R., Czerny B. 1987, MNRAS, 224, 443
- Risaliti G., et al. 2009, ApJ, 696, 160
- Ross R. R., Fabian A. C. 1993, MNRAS, 261, 74
- Ross R. R., Fabian A. C. 2005, MNRAS, 358, 211
- Róžańska A., Dumont A.-M., Czerny B., Collin S. 2002, MNRAS, 332, 799
- Saxton R. D., Read A. M., Esquej P., Freyberg M. J., Altieri B., Bermejo, D. 2008, A&A, 480, 611
- Schurch N. J., Done C., Proga D. 2009, ApJ, 694, 1
- Sim S. A., Long K. S., Miller L., Turner T. J. 2008, MNRAS, 388, 611
- Turner T. J., Miller L. 2009, A&A Review, 17, 47
- Vestergaard M., Peterson B. M. 2006, ApJ, 641, 689
- Voges W., et al. 1999, A&A, 349, 389
- Walter R., Fink H.H. 1993, A&A, 274, 105
- Zycki P. T., Krolik J. H., Zdziarski A. A., Kallman T. R. 1994, ApJ, 437, 597